MEMS Single Axis Capacitive Accelerometer

Pratham Goel

Abstract

This technical paper presents the design of a MEMS single-axis capacitive accelerometer, pivotal for safety applications like car airbag systems. Utilizing MEMS technology for precision and compactness, the design, simulated using MATLAB Simulink and Solidworks, features a differential capacitive mechanism with a focus on efficient spring-mass-damper dynamics and accurate mechanical properties modeling. The study encompasses detailed system-level analysis, ensuring optimal accelerometer performance in critical safety functions.

Introduction

In the ever-evolving field of microsystems, the integration of Micro-Electro-Mechanical Systems (MEMS) into safety-critical applications represents a pivotal step towards enhancing reliability and responsiveness. This technical paper presents a comprehensive proposal for the design of a MEMS-based accelerometer, tailored for deployment in car airbag systems during collisions. Our focus is to harness the precision and compact nature of MEMS technology to develop a device that meets stringent specifications and contributes significantly to vehicular safety.

1.
2. Accelerometer Structure and Design

MEMS diiferential capacitive accelerometer is designed and simulated using MATLAB Simulink, Solidworks Simulations and Autodesk Fusion 360. The design includes a schematic representation of the accelerometer, inclusive of its biasing mechanism, as illustrated in Figure 1.

The design features a movable proof mass, which is connected to a stationary anchor through a series of springs. Additionally, stator fingers, which are integral to the accelerometer's structure, remain fixed and are also connected to the anchor.

The operational principle of the accelerometer is akin to the classic spring-mass-damper system. This system employs a seismic mass, also known as the proof
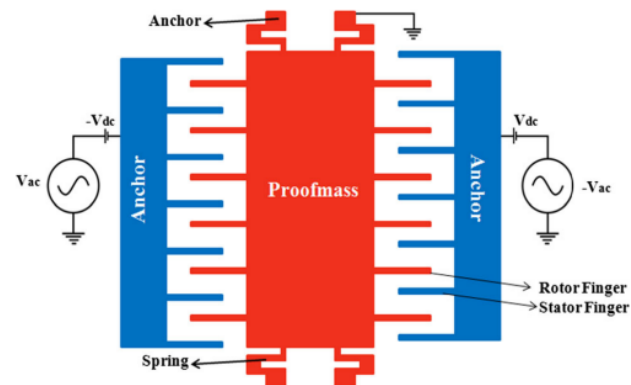

Figure 1: Schematic od MEMS accelerometer. (Mukhiya et al., 2019)

mass. Upon the application of external acceleration, this mass shifts from its equilibrium position. According to Newton's second law of motion, the sum of all forces acting on the proof mass equates to the inertial force exerted upon it. Consequently, the accelerometer's behavior can be described by a second-order differential equation (Equation 1), assuming no bias is applied to the electrodes.

$$F_{applied} = m\ddot{x} + b\dot{x} + kx = ma$$

where, m is the proofmass, b is the damping coefficient, k is the spring constant and a is applied acceleration. Hence,

$$\frac{x(s)}{a(s)} = \frac{1}{s^2 + \dfrac{b}{m}s + \dfrac{k}{m}}$$

$$T(s) = \frac{1}{(s^2 + 2\zeta\omega_{n}s + \omega_n^2)}$$

Which gives,

$$\omega_n = \sqrt{\frac{k}{m}} \rightarrow f_n = \frac{1}{2\pi}\sqrt{\frac{k}{m}}$$

where, ω_n is the natural frequency in rad/s and f_n is the natural frequency in Hz.

2.1 Spring Structure

In the context of the second-order differential equation (Equation 2), the mechanical spring stiffness (k) plays a crucial role. The spring structure, as depicted in Figure 2, is modeled using a linear approach with a Bernoulli beam

Figure 2: Spring Structure (Mukhiya et al., 2019)

element type. This model choice is made for efficient and precise simulation purposes. According to the Euler–Bernoulli beam theory, this type of element primarily accounts for stress along the beam's axis, while stress across the cross-axis is deemed negligible.

A key design consideration for this spring structure is the gap between two parallel beams. This gap is maintained at more than thrice the structure's maximum displacement. This spacing is critical to accommodate various forces, including mechanical and electrical forces, as well as thermal expansion. The design also features substantially sized anchors to securely maintain the structure's position.
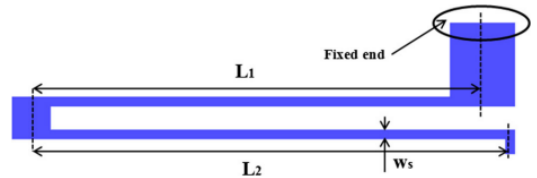
$$k = 2\left(\frac{\pi^4}{6}\left(\frac{E.t.w_s^3}{(2.L_1)^3 + (2.L_2)^3}\right)\right)$$

Where, , E represents Young's modulus, t denotes the thickness , spring constant (k), the spring's length ($L_1 \; and \; L_2$), and its width (w_s), with the series and parallel combinations of beam elements, is mathematically expressed in above Equation .For the purpose of calculating the spring constant, the lengths of L1 and L2 are considered equal.

It's important to note that the dimensions of the anchor and the smaller beam that connects the two longer beams do not significantly impact the value of the spring constant. These components are therefore considered nearly rigid (Senturia 2001). This approach simplifies the modeling process while still ensuring an accurate representation of the spring's mechanical properties.

2.2 Physical Dimensions

Figure 3. shows the schematic of the comb structure. Gap $d_1 = 13\mu m$ selected to meet the fabrication feasibility aspects.

The volume and mass of the proofmass is calculated as:

$$V = t_m(l_m.w_m + 2.N.l_c.w_c)$$
$$m = \rho V$$

Where, ρ is the density of proofmass material, V is the volume of proofmass and m is the mass value of proofmass.
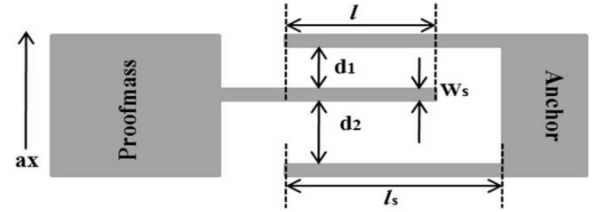
Figure 3: Comb Structure (Mukhiya et al., 2019)

In the design of MEMS accelerometers, particularly between the stator and rotor fingers, two primary damping mechanisms are identified: squeeze-film damping and Couette-flow damping. According to Chen (2010), although both exist in this context, the impact of Couette-flow damping is considerably smaller than that of squeeze-film damping. Consequently, for simplification and practicality in modeling, the effects of Couette-flow damping are often neglected.

The damping coefficient for the gaps d1 and d2, which are critical in the design of the accelerometer, can be effectively modeled using equations tailored for Hagen-Poiseuille flow. This approach is well-documented and supported by the findings in Bao and Yang (2007) and Gönenli et al. (2010). The respective equations for calculating the damping coefficients b1 and b2 are as follows:

$$b_1 = 7.2\eta_{eff}t\left(\frac{l}{d_1}\right)^3$$

$$b_2 = 7.2\eta_{eff}t\left(\frac{l}{d_2}\right)^3$$

where, η_{eff} is the effective viscosity, t is the device thickness, l is the overlap length of combs.

All the parameters are suited for in-plane proof mass motion using SOI-MUMPS technology.

Table 1: Summary Table

| Parameter	Value
Proofmass dimensions $(l_m \times w_m)$	$3500 \ \mu m \ \times 1900 \ \mu m$
Thickness (t)	$25 \ \mu m$
mass value of proof mass (m)	$4.36 \times 10^{-7} \ kg$
Comb dimensions $(l_c \times w_c)$	$850 \ \mu m \ \times 7 \ \mu m$
Overlap length (l)	$810 \ \mu m$
Spring dimensions $(l_s \times w_s)$	$750 \ \mu m \ \times 15 \ \mu m$
Spring Constant (k)	$69 \ N/m$
Quality Factor (Q)	2.94
Number of Combs on one side (N)	70
Smaller gap between comb (d_1)	$10 \ \mu m$
Larger gap between comb $(d_2))$	$30 \ \mu m$
Natural Frequency (f_n)	$2002.41 \ Hz$
Differential Capactance	$0.001 \ pF$
Capacitance with smaller gap (C_1)	$0.96 \ pF$
Capacitance with larger gap (C_2)	$0.54 \ pF$
Displacement at $40g$	$2.4 \ \mu m$

3. System-Level Analysis
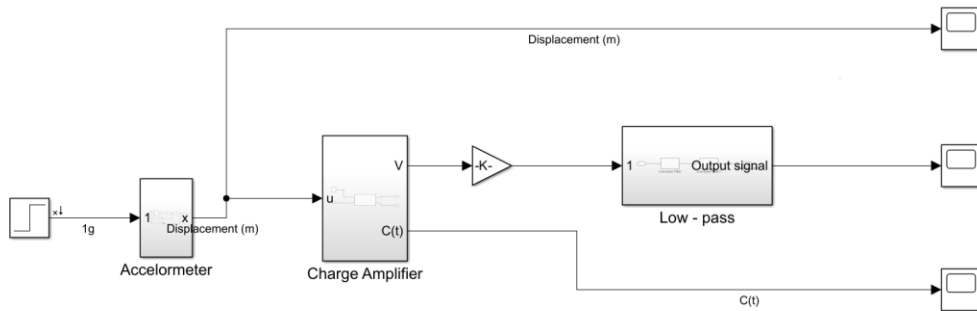
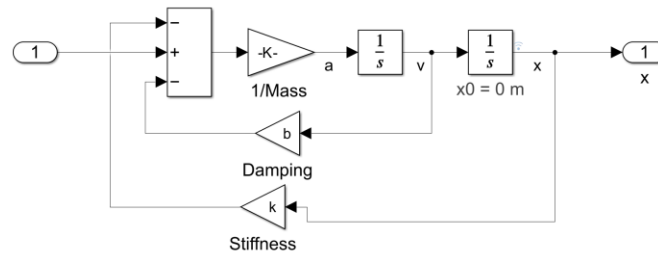*Figure 4: Information flow Analysis*

3.1 Accelerometer

Figure 5: Accelerometer Block

In our study, we present a detailed simulation of the information flow model for our MEMS accelerometer, utilizing MATLAB's Simulink. This model intricately mimics the behavior of the accelerometer's Mass-Spring-Damper system, a cornerstone in understanding its dynamic response. By representing the mass, spring, and damper through integrator and gain blocks, and aggregating forces with a sum block, we construct a simulation that precisely mirrors the physical phenomena within the accelerometer.

3.2 Charge Amplification

The Charge Amplifier Block depicts the behavior of electrical circuit shown in figure 6.

It inputs the displacement of the MEMS accelerometer and calculates the V_o. It is calculated using MATLAB function and transfer function block which also outputs the changes in capacitance w.r.t to change in displacement.

$$V_o = \frac{V_s(C_{s2} - C_{s1})}{C_1}$$
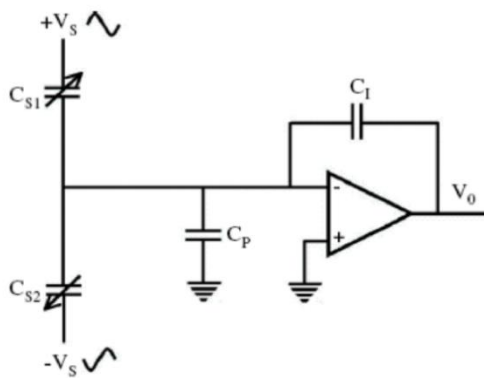
Figure 6: Charge Amplifier Circuit

Figure 7 shows the Capacitance formation in the accelerometer.
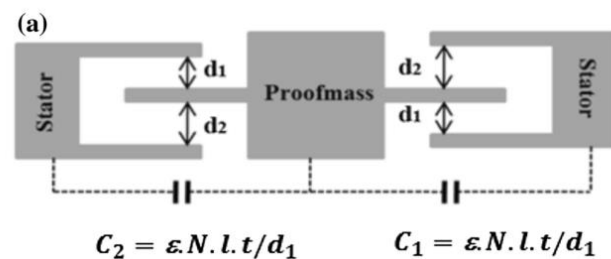

$$C_2 = \varepsilon.N.l.t/d_1 \qquad C_1 = \varepsilon.N.l.t/d_1$$

Figure 7: Charge Formation (Mukhiya et al., 2019)

$$C_1 = \frac{\varepsilon.N.l.t}{d_1 + x}$$

$$C_2 = \frac{\varepsilon.N.l.t}{d_1 - x}$$

3.3 Demodulation and filtering

The output of charge amplifier is modulated by the carrier amplitude and has to be demodulated. A gain block is added to provide gain. The output of the demodulator is filtered with low pass filter with a cut-off frequency to get change in output voltage V_o.

3.4 Results and discussion

The accelerometer is applied with 1g as step input at 0.1 s with total run of 0.5 s. the output signal and the frequency response are shown in Figure 8 and Figure 9 respectively.
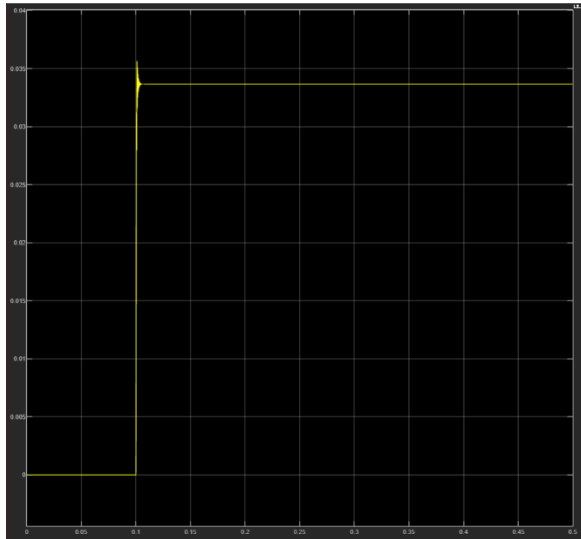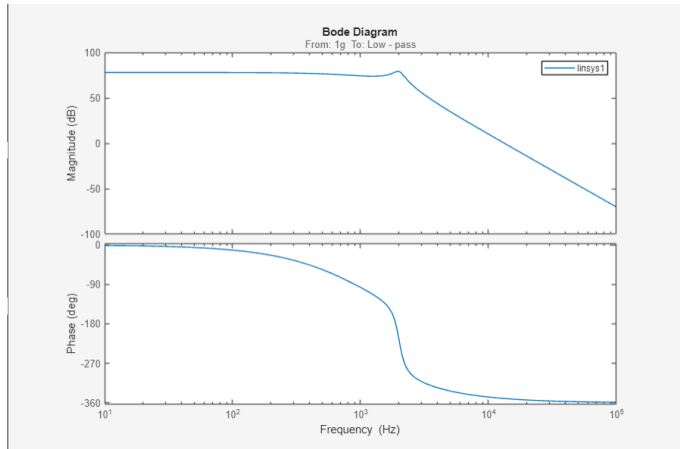

Figure 8: Time Response of 1g step input

Figure 9: Frequency Response of the Information Flow
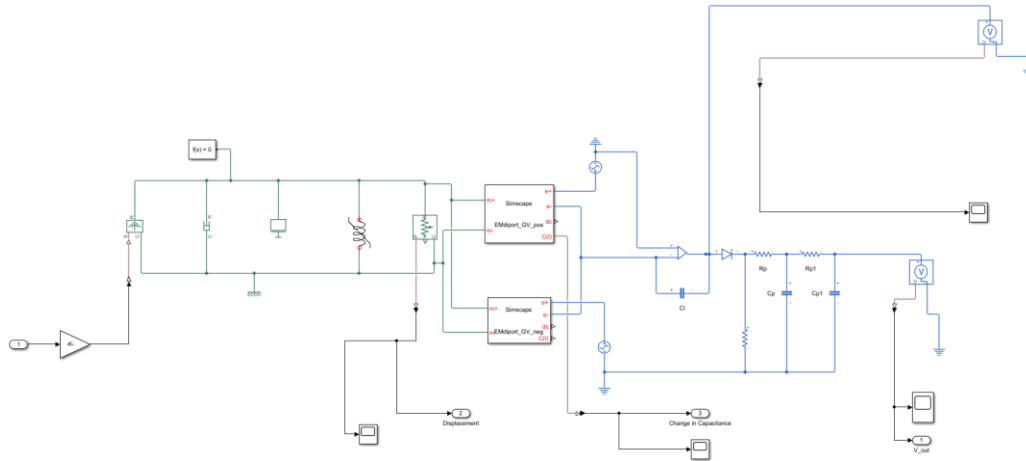
4. Energy Flow Modeling

Figure 8: Energy-flow model

Our simulation strategy revolved around the mass-spring-damper system, which is the heart of our MEMS accelerometer model. We employed an EMdiport block to meticulously compute the voltage output corresponding to mechanical movements within the system. Following this, a charge amplifier constructed using operational amplifiers was implemented to enhance the signal quality. To further refine our output, we employed a demodulation stage coupled with an RC circuit filter, effectively smoothing the signal and reducing unwanted noise. The model is Input with 1g force and low pass second RC filter was built in the circuit with cutoff frequency of 1000 Hz
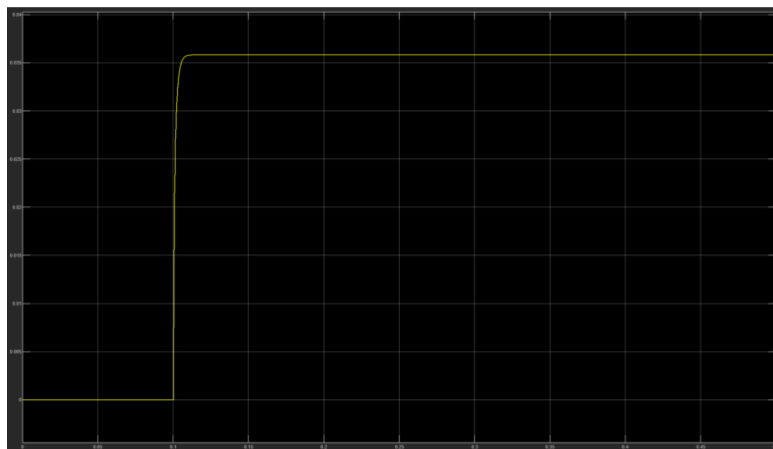
4.1 Results and Simulations

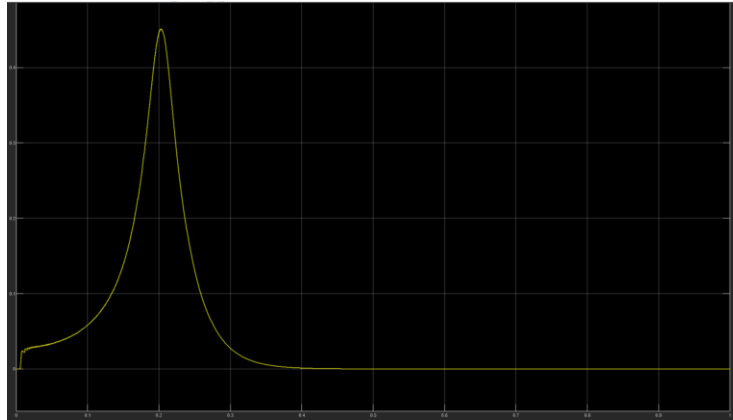*Figure 9: Output signal of Energy-Flow model for 1g step input*

Figure 10: Frequency Response of Energy Flow model with chirp Signal
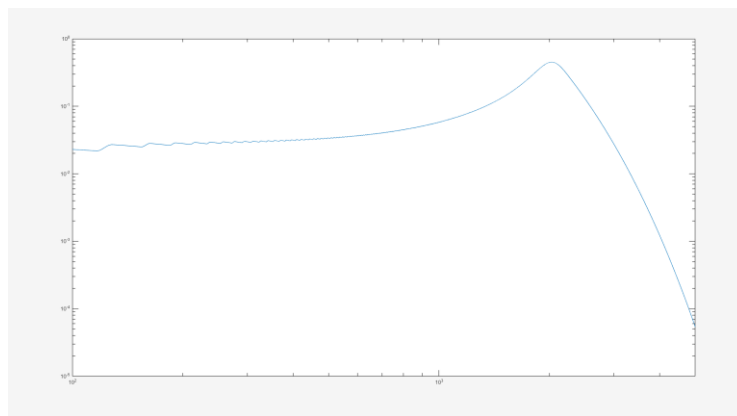

Figure 11: Bode plot of the output voltage signal.

For the frequency-response, chirp signal was input to the model and as seen in figure 10, the output voltage settles near 0.2s through which we can conclude the cutoff frequency is 1kHz. The bode plot was also calculated as shown in figure 11. Hence the model can handle signals between 0-400 Hz.

4.2 Comparison

Time Response

On comparing the time-response graphs for step 1g input it is clearly seen that the information flow shows a sudden change in the voltage signal at 0.1 s and oscillates for a while before settling down whereas in energy model, since the capacitors can hold charge, we seen a smooth increase in voltage without any oscillation. Both have max $V_o = 0.0358\ V$. The in linearity is seen because how the different model handles the signal processes.

Frequency Response

In MEMS accelerometer design, variations in time and frequency response graphs between information flow and energy flow models are expected due to their distinct analytical focuses and inherent assumptions. The information flow model concentrates on signal processing, emphasizing how the accelerometer interprets and transmits acceleration data. In contrast, the energy flow model delves into the physical dynamics of the system, such as energy storage, dissipation, and conversion. These models inherently apply different simplifications and assumptions, particularly in damping characteristics and system nonlinearities, leading to variations in the observed responses. While the information flow model may simplify mechanical aspects to prioritize electronic signal behavior, the energy flow model often provides a more detailed representation of mechanical energy dynamics. Such differences highlight the importance of employing both models for a comprehensive evaluation of the accelerometer's performance, ensuring a balanced understanding of both its physical and information processing characteristics.
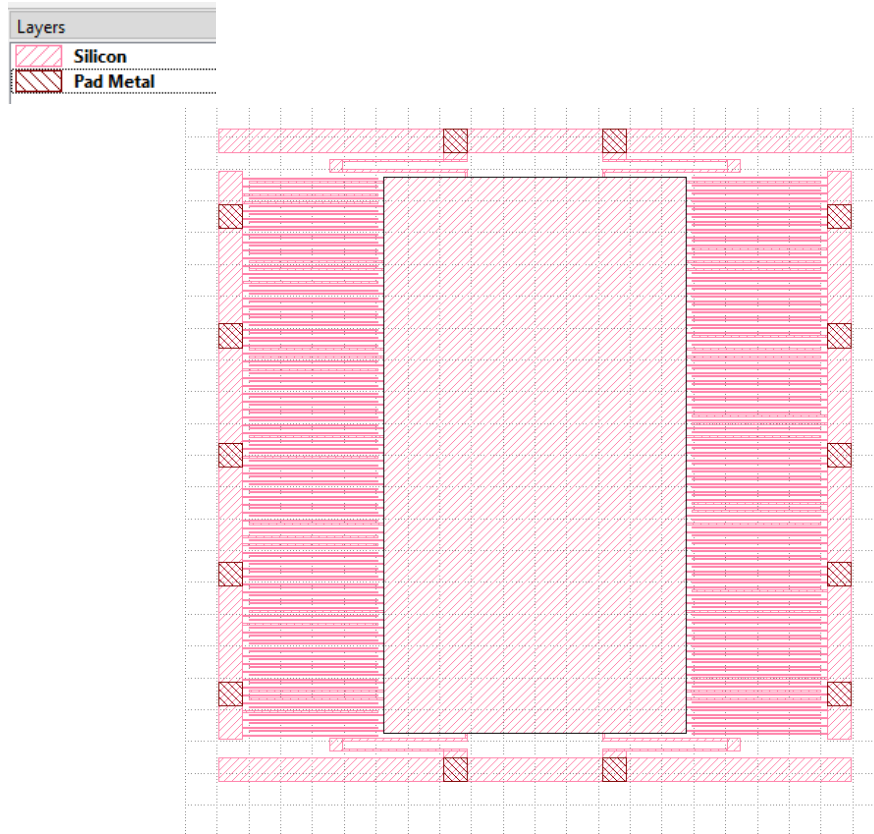
5. CAD geometry and finite Analysis

5.1 Layout Design

Figure 12: Layout design
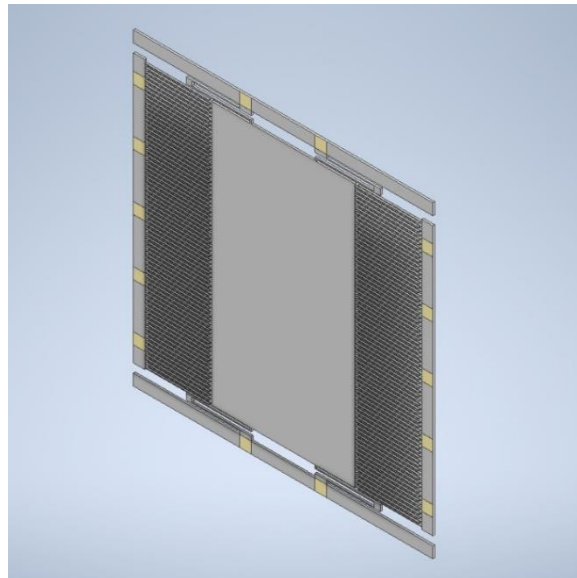
5.2 3D model

Figure 13: 3D model using Autodesk.

5.3 Finite Element Analysis

5.3.1   Static Analysis

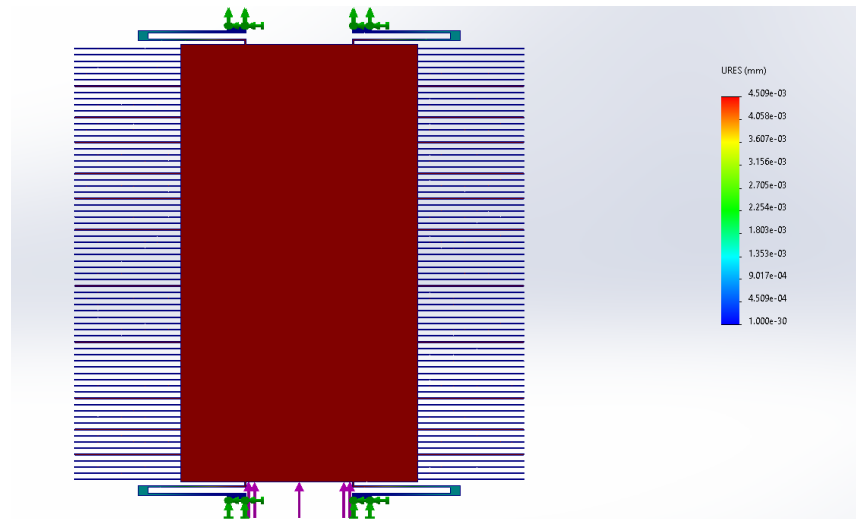Force – Displacement Static Analysis is performed using SolidWorks Simulation.

Figure 14: Static Analysis

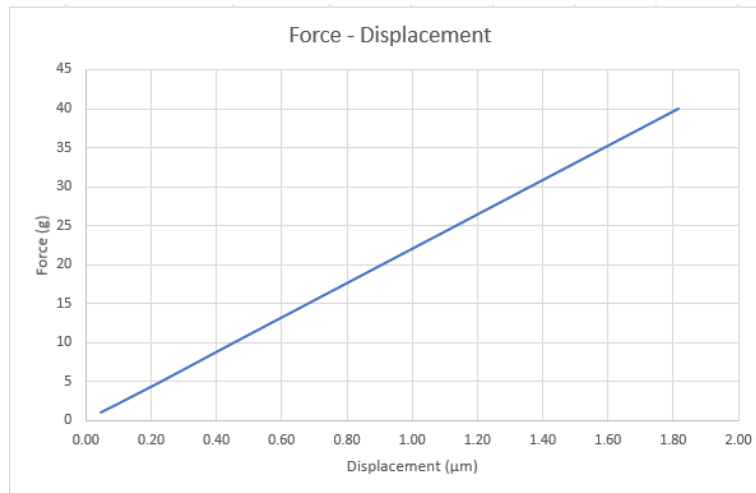| Force (g)	Displacement (μm)	$k\ (N/m)$
1	0.0451	94.9212686
2	0.0900	94.1989216
5	0.27	94.2101882
10	0.454	94.2101882
20	0.856	94.1989216
30	1.28	94.1651376
40	1.71	94.2214573

Figure 15: Force-Displacement curve

The difference in the calculated spring constant k values—94 N/m from Finite Element Analysis (FEA) versus 69 N/m from the analytical formula—can be attributed to the more detailed and comprehensive nature of FEA. While the analytical formula offers a simplified estimation based on ideal assumptions, FEA considers complex geometries, material properties, stress concentrations, potential non-linear behaviors, and other sophisticated aspects of the spring structure. This results in a more accurate and generally higher value of k with FEA, as it captures the intricacies of real-world conditions that the analytical approach may overlook.

5.3.2   Modal Analysis

Mode 1 (undeformed)

Mode 2 (deformed result)

Mode 3 (deformed result)
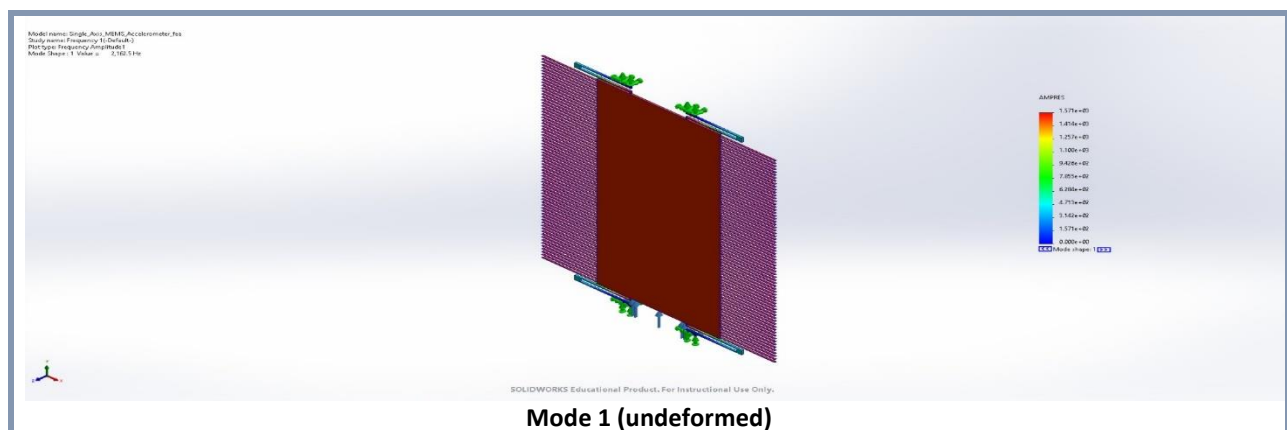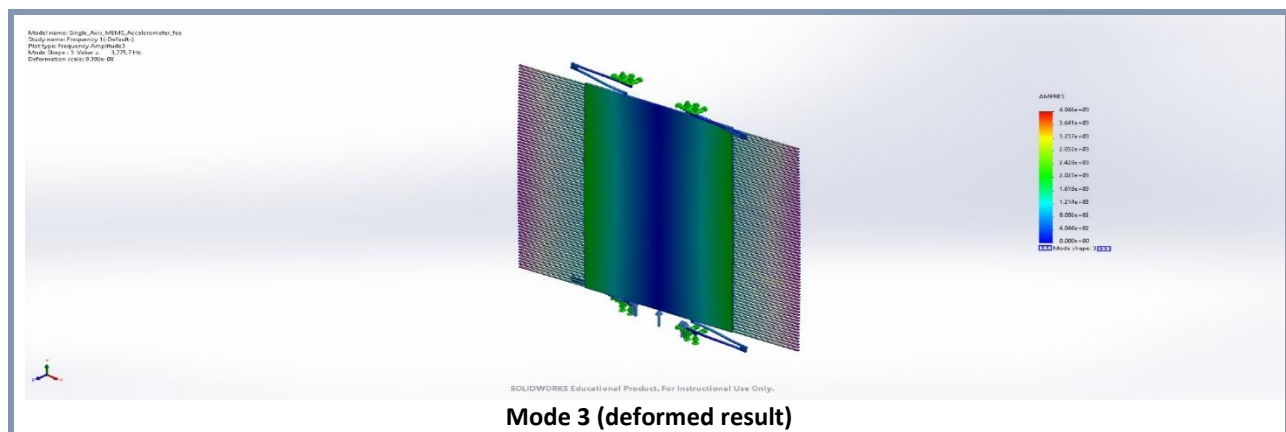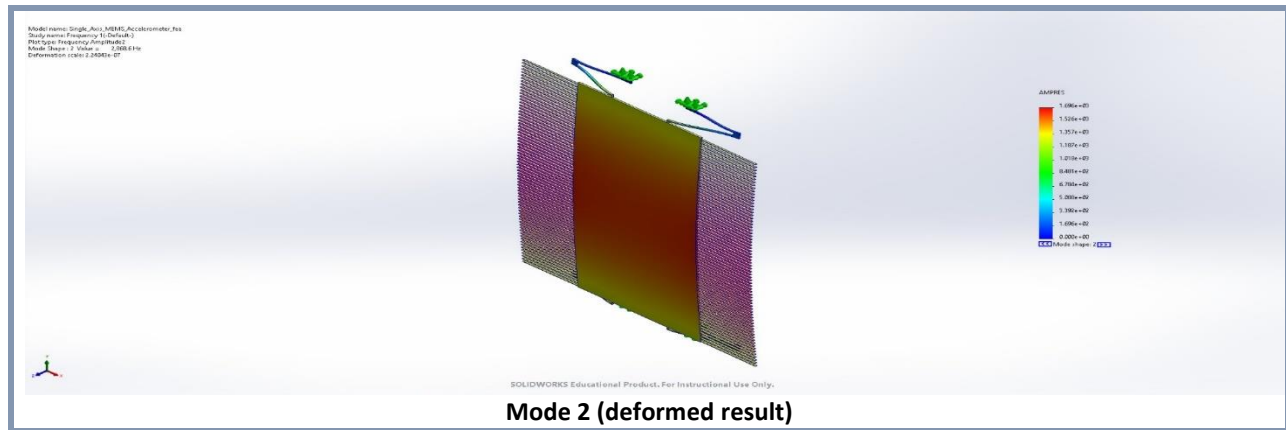
The report does not include visualizations and snapshots of the modal frequency due to the limitations imposed by the student license of SolidWorks, which restricts the inclusion of such elements.

Mode List

Frequency Number	Rad/sec	Hertz	Seconds
1	13,587	2,162.5	0.00046242
2	18,024	2,868.6	0.0003486
3	23,723	3,775.7	0.00026485

Mass Participation (Normalized)

Mode Number	Frequency(Hertz)	X direction (mm)	Y direction (mm)	Z direction (mm)
1	2,162.5	5.5945e-08	0.98989	5.7852e-06
2	2,868.6	1.8991e-07	5.8177e-06	0.98334
3	3,775.7	5.1799e-07	6.3624e-06	3.5257e-09

The table outlines the resonant mode frequencies and corresponding mass participation data for a MEMS accelerometer, revealing its sensitivity characteristics. The first resonant mode at 2,162.5 Hz shows significant mass participation in the Y direction, indicating a high sensitivity to movements in that plane at this frequency. The second and third modes, at 2,868.6 Hz and 3,775.7 Hz, respectively, show mass participation primarily in the Z direction for mode 2 and a negligible amount in the Z direction for mode 3, suggesting that the accelerometer's sensitivity is predominantly in the Z direction at these higher frequencies. These details are crucial for the design and application of the accelerometer, ensuring that its resonant frequencies align with the operational requirements of the intended measurement tasks. The relationship between resonant frequencies and mass participation effectively dictates the accelerometer's responsiveness to external accelerations, which must be carefully considered to maximize its performance and accuracy within its target frequency range.

6. Layout and mask setup.

The .gds file attached specifies the required layout, including the mask layouts. In this project, three mask layouts are utilized: SOI, PADMETAL, and TRENCH. I have opted to exclude the BLANKETMETAL in the current phase of the study. While including BLANKETMETAL could potentially improve the conductivity of the design, especially in the fingers, it is not incorporated at this stage. However, I am considering its inclusion in future developments.
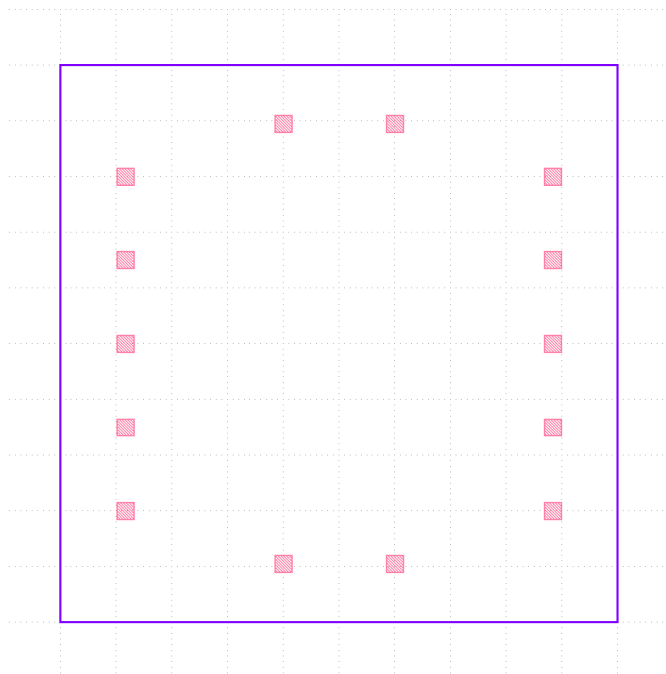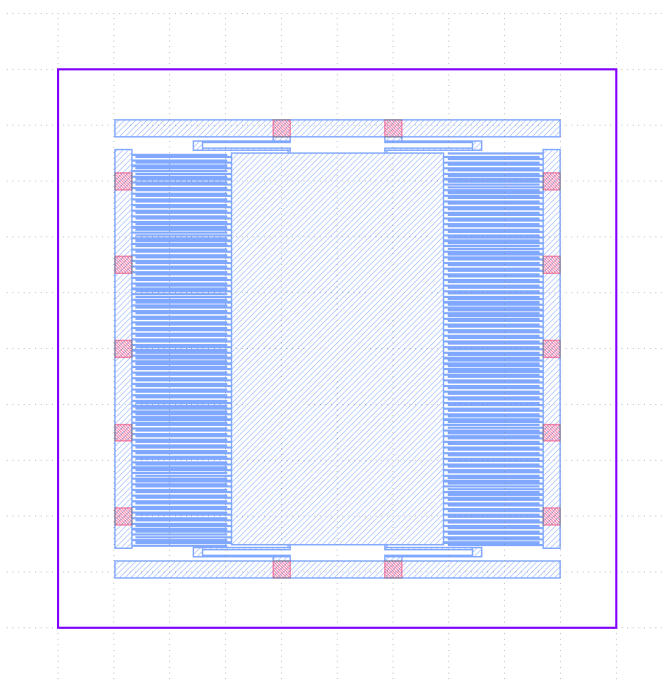
Figure 16: PADMETAL mask on 5x5 mm Silicon
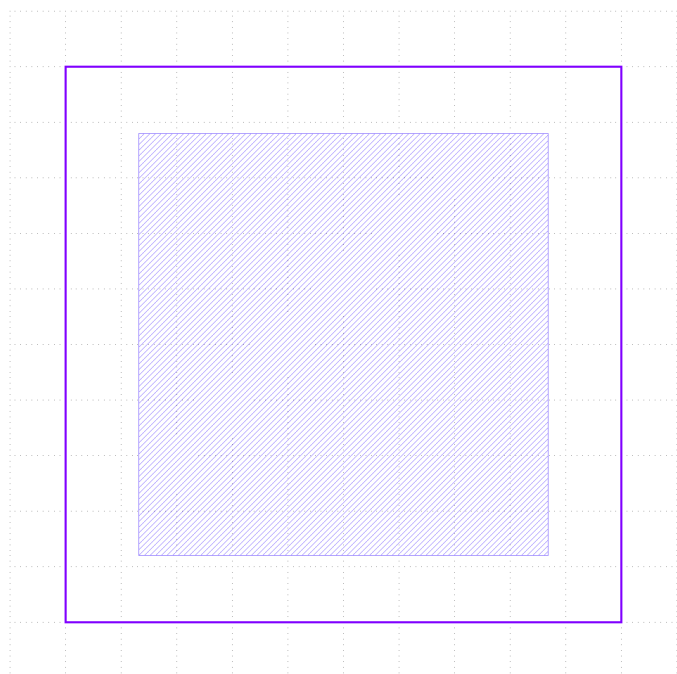

Figure 17: SOI mask with metal deposited

Figure 18: TRENCH mask

REFERENCES

Mukhiya, R., Agarwal, P., Badjatya, S., Garg, M., Gaikwad, P., Sinha, S., Singh, A. K., & Gopal, R.

(2019). Design, modelling and system level simulations of DRIE-based MEMS differential

capacitive accelerometer. *Microsystem Technologies*, *25*(9), 3521–3532.

https://doi.org/10.1007/s00542-018-04292-0